

31. W. Traeder, *Tieraerztl. Umsch.* **49**, 465 (1994).
 32. N. L. Paiva, M. F. Roberts, A. L. Demain, *J. Ind. Microbiol.* **12**, 423 (1993); P. A. S. Lowden, G. A. Böhm, J. Staunton, P. F. Leadlay, *Angew. Chem. Int. Ed. Engl.* **35**, 2249 (1996); C. G. Kim *et al.*, *J. Am. Chem. Soc.* **118**, 7486 (1996).
 33. R. McDaniel, S. Ebert-Khosla, D. A. Hopwood, C. Khosla, *Nature* **375**, 549 (1995).
 34. P. F. Leadlay, *Curr. Opin. Chem. Biol.* **1**, 162 (1997).
 35. D. A. Hopwood *et al.*, *Genetic Manipulation of Streptomyces—A Laboratory Manual* (John Innes Foundation, Norwich, UK, 1985).
 36. Supported by a project grant from the U.K. Biotechnology and Biological Sciences Research Council Biotechnology Directorate. We thank P. Skelton and J. B. Lester for assistance with, respectively, mass spectrometry and DNA sequencing; A. L. Cutter for authentic samples of triketide lactones; H. A. I. McArthur and J. Dirlam for helpful discussions; and D. Hopwood and C. Khosla for the kind provision of *S. coelicolor* CH999 and plasmid pRM5. We also wish to thank Pfizer Central Research for assistance in the scale-up and isolation of some of the novel compounds, and I. Parsons and D. M. Rescek for NMR data.

8 August 1997; accepted 24 September 1997

Femtosecond Dynamics of Electron Localization at Interfaces

N.-H. Ge, C. M. Wong, R. L. Lingle Jr.,* J. D. McNeill, K. J. Gaffney, C. B. Harris†

The dynamics of two-dimensional small-polaron formation at ultrathin alkane layers on a silver(111) surface have been studied with femtosecond time- and angle-resolved two-photon photoemission spectroscopy. Optical excitation creates interfacial electrons in quasi-free states for motion parallel to the interface. These initially delocalized electrons self-trap as small polarons in a localized state within a few hundred femtoseconds. The localized electrons then decay back to the metal within picoseconds by tunneling through the adlayer potential barrier. The energy dependence of the self-trapping rate has been measured and modeled with a theory analogous to electron transfer theory. This analysis determines the inter- and intramolecular vibrational modes of the overlayer responsible for self-trapping as well as the relaxation energy of the overlayer molecular lattice. These results for a model interface contribute to the fundamental picture of electron behavior in weakly bonded solids and can lead to better understanding of carrier dynamics in many different systems, including organic light-emitting diodes.

Polarization interactions and the localization of charge carriers in condensed media continue to represent a challenge for theoretical descriptions of the interaction of a carrier with its environment. Understanding charge localization is important in determining the electronic and optical properties of applied materials and in the development of new materials. Despite extensive study of charge localization phenomena, electron localization at interfaces between dissimilar materials, such as metal-dielectric interfaces, remains largely unexplored. Electrons in metals are usually free-electron-like, whereas electrons in dielectric solids tend to be localized as small polarons (1). Small polarons form when charges become localized in self-induced potentials as a result of strong carrier-lattice interactions (2). These self-trapped carriers and the associated lattice relaxation affect a wide range of phenomena, such as photochemical defect formation (3), atomic desorption from solid surfaces (4), and various properties of high-temperature superconducting

oxides (5). Here, we show how the transition from delocalized to localized electronic behavior near the metal-dielectric interface occurs dynamically.

The combination of recently developed angle-resolved two-photon photoemission (TPPE) (6) and femtosecond laser techniques provides a unique opportunity to study the dynamics of carrier localization at interfaces. On bare metal surfaces such as Ag(111), the image potential supports a Rydberg series of bound states characterized by the principal quantum number n with the electron density residing largely in the vacuum. Excess electrons in these image potential states are localized in hydrogenic wave functions normal to the surface, but are delocalized as plane waves parallel to the surface (7). If dielectric layers are grown on the metal substrate, one can explore the layer-by-layer evolution of the potential and the electronic structure of the interface by measuring the changes in the binding energy, effective mass, and lifetime of electrons excited into image potential states (8). With femtosecond time resolution, we can directly observe that these delocalized electrons become localized in the presence of dielectric layers. We address the underlying physical principles that lead to localization for excess electrons at multiple n -alkane layers on Ag(111).

In an angle-resolved TPPE experiment

(Fig. 1A), a pump pulse excites electrons from occupied metal states into unoccupied interfacial states, and a probe pulse ejects the excited electrons into the vacuum where the electron kinetic energy, E_{kin} , is measured at various angles, θ . From the angular dependence of the kinetic energy spectrum, one can determine both the binding energy and the effective mass, m^* , of the interfacial electrons. The relation between m^* , E_{kin} , and the electron wave vector parallel to the surface, k_{\parallel} , is given by

$$E_{\text{kin}} = \hbar^2 k_{\parallel}^2 / 2m^* + E_0 \quad (1)$$

where

$$k_{\parallel} = (2m_e E_{\text{kin}} / \hbar^2)^{1/2} \sin\theta \quad (2)$$

\hbar is Planck's constant ($\hbar = h/2\pi$), and E_0 is the kinetic energy for emission normal to the surface. An electron behaving like a free particle parallel to the interface will exhibit a dispersive band with an m^* close to the free electron mass, m_e . A spatially localized electron results in a nondispersive feature characterized by a flat energy band with a very large m^* (Fig. 1A).

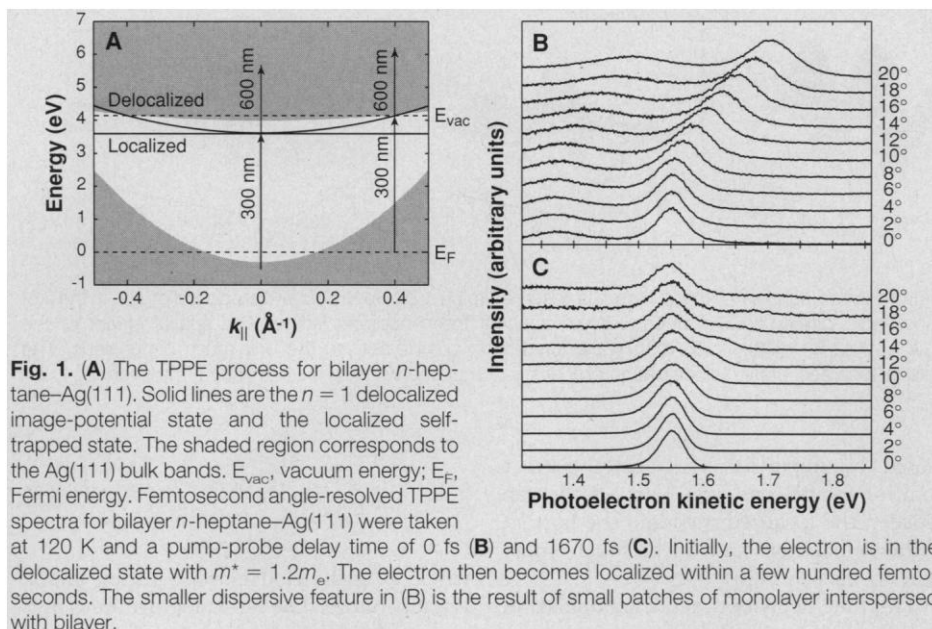
The details of the TPPE experimental apparatus have been reported in (9). In n -heptane bilayer data taken at 120 K with two different pump-probe delays, a dispersive feature with $m^* = 1.2 m_e$ appears at zero time delay (Fig. 1B), whereas a nondispersive feature appears in the spectra taken at a 1670-fs delay (Fig. 1C). These two features correspond, respectively, to the delocalized and localized states (10). The femtosecond TPPE data clearly reveal a delay in the formation of the localized state. Similar behavior is found for a monolayer and a trilayer. Lingle *et al.* studied various alkane-Ag(111) interfaces (10), investigating the effects of different preparation methods and annealing procedures on localization, and found no significant effects. In addition, the proportion of monolayer patches interspersed with bilayer (apparent in Fig. 1B) can be varied without variation in the bilayer dynamics. These experiments indicate that the observed localization phenomenon and dynamics are not controlled by defects in the layer, but rather are linked to the intrinsic two-dimensional (2D) properties of the layer.

We measured the dynamics of the localized and delocalized features at 120 K for various angles (Fig. 2). The delocalized fea-

Department of Chemistry, University of California, Berkeley, CA 94720, USA, and Chemical Sciences Division, Lawrence Berkeley National Laboratory, Berkeley, CA 94720, USA.

*Present address: Lucent Technologies, Bell Laboratories, 2000 Northeast Expressway, Norcross, GA 30071, USA.

†To whom correspondence should be addressed. E-mail: harris@socrates.berkeley.edu



ture (Fig. 2A) decays more quickly than the localized feature (Fig. 2B). Extraction of the rise and decay times shows that, within the 95% confidence limit, the localized feature exhibits the same rise time (360 ± 140 fs) and decay time (1600 ± 200 fs) over the range of angles studied. In contrast, the dynamics of the delocalized states have a strong angle dependence. The rise times vary from 780 ± 390 fs ($k_{\parallel} = 0$) to 70 ± 30 fs ($k_{\parallel} = 0.23 \text{ \AA}^{-1}$), and the decay times range from 810 ± 210 to 200 ± 50 fs, respectively.

A spatially localized state can be considered as a superposition of many k_{\parallel} plane waves in the band (Fig. 3, point C). The energy expended, termed the localization energy, E_{loc} , can be estimated from the half width of the band, B (12). On the other hand, localization through small-polaron formation is encouraged, because the electron can create for itself an attractive potential well by polarizing and displacing the atoms surrounding it (Fig. 3, point S), thus releasing the lattice relaxation energy, E_{rel} . The localized or self-trapped state of the electron will be energetically more favorable, and the small polaron will form when the self-trapping energy, E_{st} , is positive:

$$E_{st} = E_{rel} - E_{loc} > 0 \quad (3)$$

For the delocalized states, however, both the magnitudes and the k_{\parallel} dependence of the lifetimes (Fig. 2A) suggest that decay mechanisms other than tunneling are operative. The rise time of the localized state is within the range of the decay time of the delocalized state. In fact, they correspond even at different temperatures. As the temperature is lowered from 120 to 50 K, both rates become faster. Also, the time-integrated intensity of the localized state is similar to that of the delocalized state. These strong correlations between them indicate that the delocalized electrons primarily decay into the localized state. As shown below, these data are well explained by a 2D small-

polaron model for localization, and the k_{\parallel} dependence of the decay times of the delocalized states is related to the lattice relaxation dynamics, which lead to self-trapping.

Small-polaron formation is conceptually simple. An electron in a crystal is subject to a competition between delocalizing and localizing tendencies (11). Delocalization is favored because an electron residing at the bottom of a band has low kinetic energy (Fig. 3, point F). In order to localize the electron at a single site without lattice distortion, energy is required to construct an electron wave packet from all Bloch waves in the band, termed the localization energy, E_{loc} , can be estimated from the half width of the band, B (12). On the other hand, localization through small-polaron formation is encouraged, because the electron can create for itself an attractive potential well by polarizing and displacing the atoms surrounding it (Fig. 3, point S), thus releasing the lattice relaxation energy, E_{rel} . The localized or self-trapped state of the electron will be energetically more favorable, and the small polaron will form when the self-trapping energy, E_{st} , is positive:

The energy difference of ≤ 10 meV between the bottom of the parabolic band (Fig. 1B, 0°) and the localized state (Fig. 1C) is a measure of E_{st} and is found to be independent of layer thickness, even though the binding energy of the delocalized state changes with layer thickness. The invariance of E_{st} versus layer thickness suggests that the localization process observed is associated with interactions between the electron and the topmost plane of the al-

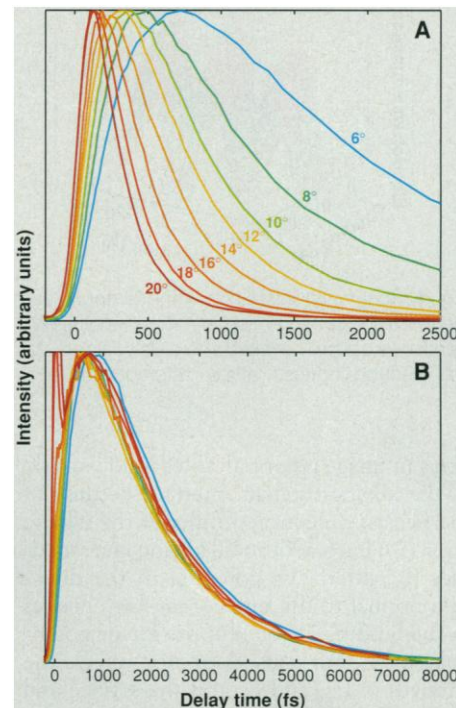


Fig. 2. Ultrafast time-resolved TPPE traces for (A) the delocalized and (B) the localized state for bilayer *n*-heptane on Ag(111) at various angles and 120 K. The spikes near time zero in (B) for data at high angles come from short-lived electrons on small patches of monolayer.

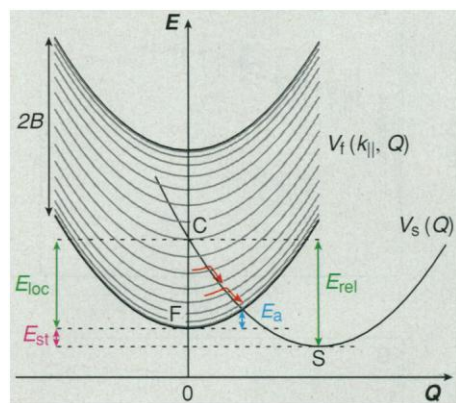


Fig. 3. Configuration coordinate diagram for self-trapping of an electron. Curves $V_f(k_{\parallel}, Q)$ and $V_s(Q)$ are associated, respectively, with the free states (without electron-phonon coupling) and the self-trapped state. The quantity Q is the phonon coordinate responsible for self-trapping. Each curve in the V_f manifold represents a different k_{\parallel} state with a band energy E_{\parallel} ($E_{\parallel} = 0$ at $k_{\parallel} = 0$). The width of the band ($2B$), localization energy (E_{loc}), lattice relaxation energy (E_{rel}), self-trapping energy (E_{st}), and the activation energy of self-trapping (E_a) for $k_{\parallel} = 0$ are depicted. Red arrows indicate the classical barrier crossing from the delocalized to the localized state.

kane molecules without rearrangement of the layer below. This picture of 2D interactions is consistent with the fact that elec-

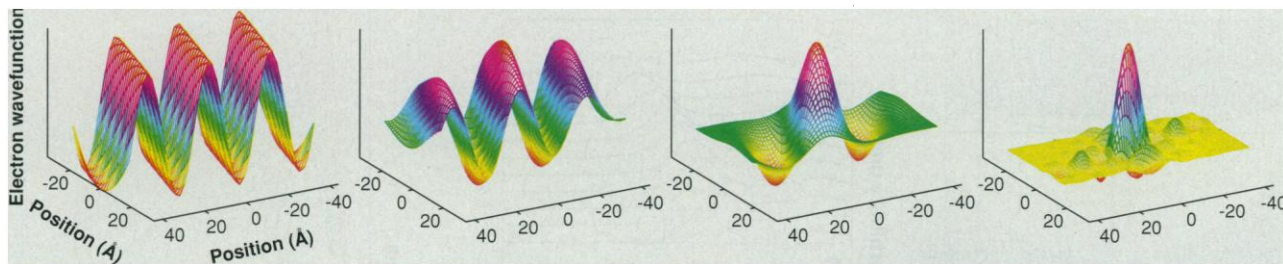


Fig. 4. Schematic illustration of the temporal evolution (from left to right) of the electron wave function at the *n*-heptane-Ag(111) interface. Initially, an electron is optically excited into a delocalized state with $k_{\parallel} = 0.22 \text{ \AA}^{-1}$ (left). The electron induces lattice distortion and evolves into a localized state (right), which is assumed to be a 2D wave packet composed of all k_{\parallel} in the first surface Brillouin zone of the *n*-heptane lattice. The spatial extent of the resulting wave function is comparable to the unit mesh dimensions. The localization process is completed within a few hundred femtoseconds.

trons in image potential states reside mostly at the alkane-vacuum interface because of the negative electron affinity of the alkane layer (9). Each additional alkane layer modifies the interfacial potential in the direction normal to the surface, causing changes in the binding energies of the image potential states, but this does not affect the strength of E_{rel} and E_{loc} on the surface and leaves E_{st} unchanged. Furthermore, the small value of E_{st} is consistent with predictions for a 2D system (11, 13). Impurity-enhanced localization can be ruled out from the fact that E_{st} is small. If localization were

caused by impurities chemically distinct from *n*-heptane, one would expect the gap between the localized state and the bottom of the delocalized band to be much larger than 10 meV.

The time delay between the population of the image state and the formation of the localized electrons is a manifestation of the dynamic aspect of small-polaron formation. The initial creation of delocalized electrons on the surface (Fig. 1B) is a consequence of the Franck-Condon principle (14). The excited electrons can then be stabilized by self-trapping and become localized on a time scale associated with lattice and molecular motion (Fig. 1C). The temporal evolution of this localization process is schematically illustrated in Fig. 4. The delocalized electron wave packet evolves into a self-trapped state with a spatial extent comparable to the lattice constants of the adlayer surface mesh (15).

By inspecting the potential surfaces of the free and self-trapped states (Fig. 3) and making an analogy between electron self-trapping processes and electron transfer reactions (16), one can understand and quantitatively model the strong k_{\parallel} dependence of the self-trapping rate (Fig. 2A). A self-trapping process that starts from an initial state of particular k_{\parallel} with band energy E_{\parallel} and then proceeds to the self-trapped state corresponds to an electron transfer reaction with exothermicity of $-\Delta\epsilon \equiv E_{\parallel} + E_{\text{st}}$ (17). The extent of the mixing between the initial and final states at the crossing point is determined by the matrix element, H_{fs} , which represents the electronic coupling of the two states. Within the harmonic oscillator approximation, the activation energy or self-trapping barrier shows a quadratic dependence on $\Delta\epsilon$, being large at $k_{\parallel} = 0$, decreasing with k_{\parallel} until $-\Delta\epsilon = E_{\text{rel}}$ (point C in Fig. 3 where there is no barrier), and then turning around to increase with k_{\parallel} . The associated rate in the nonadiabatic limit ($H_{fs} \ll k_B T$) is (16, 18) given by

$$k_{\text{st}} = \sqrt{\frac{\pi}{\hbar^2 E_{\text{rel}} k_B T}} H_{fs}^2 e^{-(\Delta\epsilon + E_{\text{rc}})^2 / 4E_{\text{rc}} k_B T} \quad (4)$$

where k_B is the Boltzmann constant and T is temperature. The self-trapping rate is thus expected to initially increase with k_{\parallel} and then decrease, which gives rise to the so-called Marcus inverted region (19). The rate at which the self-trapped electrons form will be an averaged sum over self-trapping rates from all k_{\parallel} states.

The model discussed above treats the nuclear motion classically, a valid approach in the high-temperature limit. At lower temperatures, the quantum-mechanical nature of nuclear tunneling needs to be taken into account. For small-polaron formation in a molecular lattice, the electron can interact with both intra- and intermolecular vibrations, forming molecular and lattice polarons, respectively. In our temperature range, the low-frequency intermolecular vibrations can be treated classically, whereas the high-frequency intramolecular modes are frozen and require a quantum-mechanical treatment. The model we adopt here assumes that a single quantum-mechanical intramolecular mode of energy $\hbar\omega_q$ is rearranged by electron self-trapping with a reorganization energy E_{rq} (the classical intermolecular modes have a reorganization energy E_{rc}). We analyzed the data in terms of a recently developed path integral approach (20), which includes all perturbation orders in the electronic coupling H_{fs} ; the result of this analysis is shown in Fig. 5A (21). The first-order term in the path integral is an exact expression for a quantum nonadiabatic process, and it accounts for nearly 96% of the fit in Fig. 5A. That is, this process at 120 K is reasonably well described by the nonadiabatic theory (22). For a comparison to the classical theory for nuclear motion, we also fit the data with Eq. 4. A good fit is obtained only by making temperature an adjustable parameter. However, the resulting temperature, 280 K, is significantly higher than our experimental

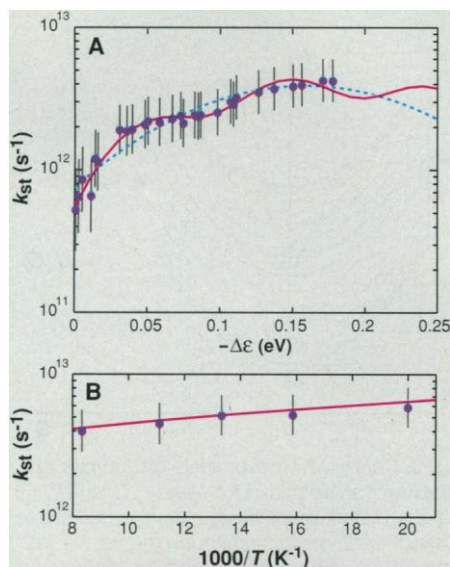


Fig. 5. (A) Logarithmic plot of the self-trapping rate of the delocalized state versus exothermicity for a bilayer at 120 K. The 95% confidence limit is indicated by the vertical line associated with each data point. The solid red line was computed by quantum theory (20) with the parameters $H_{fs} = 91 \text{ cm}^{-1}$, $E_{\text{rc}} = 0.057 \text{ eV}$, $E_{\text{rq}} = 0.18 \text{ eV}$, and $\hbar\omega_q = 750 \text{ cm}^{-1}$. The dashed blue line was computed by classical theory (Eq. 4) with the parameters $H_{fs} = 77 \text{ cm}^{-1}$, $E_{\text{rel}} = 0.16 \text{ eV}$, and $T = 280 \text{ K}$. (B) Temperature dependence of self-trapping rates for a bilayer at 18° ($k_{\parallel} = 0.21 \text{ \AA}^{-1}$). The solid line was computed by quantum theory with $-\Delta\epsilon = 0.14 \text{ eV}$ and the same parameters as in (A).

temperature, 120 K. Therefore, we conclude that the formation of the 2D small polaron is governed by quantum dissipative processes such as tunneling, and the classical theory is not applicable to this system.

It is encouraging that the parameters extracted from the fit (legend to Fig. 5A) are consistent with known values for polarons in other molecular solids: E_{rc} is consistent with the dynamic modulation of the polarization energy (~ 0.03 eV) for electron-phonon interaction in organic crystals, and E_{rq} is similar to the effective formation energy (0.15 eV) of a molecular polaron in polyacene crystals (23). The lattice relaxation energy ($E_{rel} = E_{rc} + E_{rq}$) is comparable to the localization energy E_{loc} (24), and hence, the self-trapping energy (Eq. 3) is small for this system. The energy of $\hbar\omega_q$ corresponds to an in-phase methylene rocking mode of *n*-heptane (25). The oscillatory dependence of k_{st} on $-\Delta\epsilon$ (Fig. 5A) is reproduced. The first maximum corresponds to the usual classical inverted region resulting from the intermolecular modes ($-\Delta\epsilon = E_{rc}$). Subsequent maxima originate from a resonant effect resulting from the excitation of the intramolecular mode (26) and the interval between maxima is $\hbar\omega_q$ (see Fig. 5A). Finally, with the use of the above parameters and path integral theory, the temperature dependence of k_{st} is reproduced with no other adjustable parameters (Fig. 5B). The non-Arrhenius behavior results from nuclear tunneling in the high-frequency mode.

Our results demonstrate that the ability to both time- and angle-resolve the dynamics of electrons at interfaces allows a quantitative determination of the relaxation energies and lattice displacements associated with the small-polaron self-trapping process. Our results provide an experimental basis for further theoretical studies. Time- and angle-resolved TPPE is a powerful probe for 2D electron localization and should also be applicable to a wide variety of interfaces.

REFERENCES AND NOTES

- For reviews, see A. L. Shluger and A. M. Stoneham, *J. Phys. Condens. Matter* **5**, 3049 (1993); K. S. Song and R. T. Williams, *Self-Trapped Excitons* (Springer-Verlag, Berlin, 1993).
- L. D. Landau, *Phys. Z. Sowjetunion* **3**, 664 (1933); E. I. Rashba, *Opt. Spektrosk.* **2**, 75 (1957); Y. Toyozawa, *Prog. Theor. Phys.* **26**, 29 (1961).
- W. Hayes and A. M. Stoneham, *Defects and Defect Processes in Nonmetallic Solids* (Wiley, New York, 1985).
- A. R. Burns, E. B. Stechel, D. R. Jennison, Eds., *Desorption Induced by Electronic Transitions* (Springer-Verlag, Berlin, 1993).
- J. G. Bednorz and K. A. Müller, *Z. Phys. B* **64**, 189 (1986); D. Mihailovic et al., Eds. *Anharmonic Properties of High-Tc Cuprates* (World Scientific, Singapore, 1995).
- K. Giesen, F. Hage, F. J. Himpsel, H. J. Riess, W. Steinmann, *Phys. Rev. Lett.* **55**, 300 (1985). For a review, see Th. Fauster and W. Steinmann, in *Photonic Probes of Surfaces*, P. Halevi, Ed. (Elsevier, Amsterdam, 1995), pp. 347–411. For a study of coherence phenomena, see U. Höfer et al., *Science* **277**, 1480 (1997).
- P. M. Echenique and J. B. Pendry, *Prog. Surf. Sci.* **32**, 111 (1990).
- D. F. Padowitz, W. R. Merry, R. E. Jordan, C. B. Harris, *Phys. Rev. Lett.* **69**, 3583 (1992).
- R. L. Lingle Jr., N.-H. Ge, R. E. Jordan, J. D. McNeill, C. B. Harris, *Chem. Phys.* **205**, 191 (1996); *ibid.* **208**, 297 (1996).
- R. L. Lingle Jr., D. F. Padowitz, R. E. Jordan, J. D. McNeill, C. B. Harris, *Phys. Rev. Lett.* **72**, 2243 (1994). In that paper, both localized and delocalized state appeared to coexist when studied with 6-ps time resolution.
- Y. Toyozawa, in *Relaxation of Elementary Excitations*, R. Kubo and E. Hanamura, Eds. (Springer-Verlag, Berlin, 1980), pp. 3–18; A. J. Fisher, W. Hayes, D. S. Wallace, *J. Phys. Condens. Matter* **1**, 5567 (1989).
- T. L. Gilbert, *Lecture Notes for NATO Summer School in Solid State Physics*, Ghent, Belgium (1966) [unpublished, referenced in (1)].
- D. Emin and T. Holstein, *Phys. Rev. Lett.* **36**, 323 (1976); Y. Toyozawa and Y. Shinozuka, *J. Phys. Soc. Jpn.* **48**, 472 (1980); H. Sumi, in *Excitonic Processes in Condensed Matter*, Proc. SPIE 2362, J. Singh, Ed. (SPIE, Bellingham, WA, 1995), pp. 108–119.
- That is, optical excitation primarily promotes electrons from delocalized metal states into delocalized image-potential states without lattice distortion.
- L. E. Firment and G. A. Somorjai, *J. Chem. Phys.* **69**, 3940 (1978).
- R. A. Marcus and N. Sutin, *Biochim. Biophys. Acta* **811**, 265 (1985); J. Ulstrup, *Charge Transfer Processes in Condensed Media* (Springer-Verlag, Berlin, 1979).
- Exothermicity $-\Delta\epsilon$ is determined by the photoelectron kinetic energy difference between the delocalized and localized states (see Fig. 1, B and C).
- T. Holstein, *Ann. Phys.* **8**, 325 (1959); *ibid.*, p. 343.
- R. A. Marcus, *J. Chem. Phys.* **24**, 966 (1956).
- A. A. Stuchebrukhov and X. Song, *ibid.* **101**, 9354 (1994).
- In this analysis, we attributed the decay rate of the delocalized state (after subtracting a rate for tunneling back into the metal which is independent of $k_{||}$) to self-trapping. We ignored the possible contribution from intraband relaxation by way of electron-phonon scattering for the following reasons. First, a perturbation calculation of the rate of scattering against 2D acoustic phonons of the alkane layers did not give reasonable agreement with the energy dependence of the decay rate of delocalized states. Second, delocalized states at 50 K decay faster than at 120 K, contradicting the scattering theory prediction. However, scattering may play a role in causing the finite rise time of the delocalized state. It may also be related to the similar dynamics recently observed in the neopentane-Ag(111) system. Further studies are required to address these issues.
- However, at 50 K, the first-order term accounts for only 83% of the rate.
- E. A. Silinsh and V. Capek, *Organic Molecular Crystals: Interaction, Localization, and Transport Phenomena* (AIP Press, New York, 1994).
- Within the isotropic 2D tight-binding approximation, the half width of the delocalized band B can be estimated from m^* by $B = 2\hbar^2/m^*a^2$, where a is the lattice constant. The measured $m^* = 1.2m_e$ is an average value over *n*-heptane domains grown on the threefold symmetric Ag(111) with domain axes rotated by 120° . For a crude estimate of B , we assume a square lattice with the area of *n*-heptane surface mesh (15). Therefore, we obtained $E_{loc} \sim 0.25$ eV.
- R. G. Snyder, *J. Chem. Phys.* **47**, 1316 (1967).
- S. Efrima and M. Bixon, *Chem. Phys.* **13**, 447 (1976).
- We thank X. Song for helpful discussions. Supported by the Director, Office of Energy Research, Office of Basic Energy Sciences, Chemical Sciences Division of the U.S. Department of Energy, under contract DE-AC03-76SF00098. Specialized equipment used in some experiments described herein was supported by NSF.

21 August 1997; accepted 3 November 1997

Photonic Channels for Quantum Communication

S. J. van Enk, J. I. Cirac, P. Zoller

A general photonic channel for quantum communication is defined. By means of local quantum computing with a few auxiliary atoms, this channel can be reduced to one with effectively less noise. A scheme based on quantum interference is proposed that iteratively improves the fidelity of distant entangled particles.

Security for communication of sensitive data over public channels such as the Internet is indispensable nowadays. Quantum mechanics offers the possibility of storing, processing, and distributing information in a proven secure way by exploiting the fragility of quantum states and the fact that they cannot be cloned (1). In practice, many obstacles stand in the way of implementing a reliable quantum network. Although remarkable progress has recently been made experimentally in the context of

quantum cryptography and computation (2), the presence of errors during the transmission and processing of quantum information remains as the main obstacle. In principle, these problems could be circumvented with ingenious schemes for purifying states (3) and correcting errors (4), because they allow the transmission of intact quantum states even in the presence of errors. These "standard" methods require a large (in principle, infinite) number of extra quantum bits (qubits) to store intermediate information. However, in the first generations of experiments on quantum networks, one expects to be able to store and manip-

Institut für Theoretische Physik, Universität Innsbruck, Technikerstrasse 25, A-6020 Innsbruck, Austria.